Draft version August 9, 2013
Preprint typeset using LaTeX style emulateapj v. 04/17/13

ON MAGNETIC DYNAMOS IN ULTRACOOL DWARFS: AN INVERSE CORRELATION BETWEEN X-RAY ACTIVITY AND ROTATION

B. A. Cook[1], P. K. G. Williams[2], and E. Berger[2]

Draft version August 9, 2013

ABSTRACT

Dynamo action in fully-convective stars is currently not well-understood. The role that rotation plays in driving magnetic activity is particularly unclear, both from a theoretical standpoint, concerning how much influence stellar rotation has on the turbulent dynamo; and observationally, concerning the continuing validity of well-established empirical rotation-activity relations in solar-type stars. Although the data suggest that empirical relations between X-ray activity and other parameters, such as rotation or radio activity, change dramatically in the ultracool dwarf (UCD; defined here as objects with spectral types M6.5 or later) regime, the limited number of X-ray detections has prevented the drawing of firm conclusions. In this paper, we analyze the X-ray activity-rotation relation in 33 ultracool dwarfs. Our sample represents the largest catalog of X-ray active ultracool dwarfs to date, including new *Chandra* observations of eight late-M dwarfs and four previously-unpublished measurements from the *Chandra* archive, the reductions for three of which are detailed here. We identify a substantial number of rapidly-rotating UCDs with X-ray activity as far as two orders of magnitude below the expected saturation level and find a significant anticorrelation between rotation and X-ray activity, suggestive of a "supersaturation" effect. We discuss several mechanisms which have been proposed to explain supersaturation, including "centrifugal stripping" of X-ray emitting coronae, and find many of them to be inconsistent with the observed trends. Rather than a direct supersaturation mechanism, an unobserved parameter, weakly correlated with both X-ray activity and rotation, may be responsible for the anticorrelation. The strength and topology of large-scale stellar magnetic fields have been found to vary widely within UCDs of similar stellar parameters, and we speculate that the bimodality of field topologies could explain the observed trends. Large-scale, dipolar fields could inflate the coronae of UCDs, increasing the X-ray emitting volume while simultaneously enhancing the effects of magnetic braking compared to UCDs with tangled, multipolar fields.

Keywords: stars: low mass — stars: magnetic fields — stars: rotation — stars: activity

1. INTRODUCTION

1.1. *Magnetic Fields in Solar-Type Stars*

Stellar magnetic fields can be detected or inferred through several methods, probing different scales and properties of the magnetic field. Observations of Zeeman broadening — the broadening of spectral lines under the influence of the Zeeman effect — are sensitive to the averaged surface magnetic flux (Reiners & Basri 2006, 2008, 2010). The related Zeeman-Doppler imaging technique — in which time-resolved spectropolarimetry probes the spatial dependence of the magnetic field — can constrain the large-scale field orientation and topology (Semel 1989; Donati et al. 2006; Morin et al. 2008, 2010). These *direct* magnetic field measurement techniques are limited to slowly-rotating targets, so that Doppler broadening does not overshadow Zeeman broadening and adequate signal-to-noise can be achieved in the spectropolarimetric data.

Stellar magnetism can also be traced indirectly with observations of X-ray, Hα, and radio emission. Stellar coronae, heated to temperatures above 10^6 K through poorly understood mechanisms, are studied by their X-ray emission. Mildly relativistic particles in the corona, accelerated in magnetic reconnection events, produce nonthermal gyrosynchrotron radiation (Güdel 2002). Hα emission traces heating of the chromosphere, another poorly-understood phenomenon that is typically taken to result from a combination of X-ray heating from the corona and kinetic heating by electrons ejected in flares from magnetic reconnection (Güdel et al. 1996; Forbrich et al. 2011).

These *magnetic activity tracers* reflect how the magnetic field interacts with different parts of the stellar atmosphere. Despite the fact that they are each coupled to very different atmospheric regions and emission processes therein, some of them have been found to obey striking correlations. Güdel & Benz (1993) and Benz & Güdel (1994) discovered a power-law relation between X-ray and radio luminosity in active solar-type (F–K) stars. Solar flares have also been found to obey this relation. Including solar flare measurements with stellar data yields a strong correlation over ten orders of magnitude in radio luminosity. The similarities in the X-ray/radio ratios between solar flares and active stars suggest a common mechanism between the two. It has been proposed that "quiescent" emission in active stars is made up of contributions from many small flares across the stellar surface (Benz & Güdel 1994; Forbrich et al. 2011). The relation between various magnetic activity indicators is further supported by the Neupert effect (Neupert 1968), an observed correlation between the rate-of-change of X-

[1] Department of Astrophysical Sciences, Princeton University, Princeton, NJ, 08544. Contact email: bacook@princeton.edu
[2] Harvard-Smithsonian Center for Astrophysics, 60 Garden St., Cambridge, MA, 02138.

ray activity and radio emissivity that represents a major piece of evidence for the flaring model of chromospheric heating (Cram 1982; Benz & Güdel 1994; Güdel et al. 1996).

Magnetic activity is also correlated with stellar rotation and age. For slowly rotating (rotation velocity $v \lesssim 10$–15 km s^{-1}, dependent on spectral type) active stars of many spectral types, X-ray, Hα, and radio luminosity have all been found to correlate strongly with rotation period and velocity (or $v \sin i$, the radial component measured by Doppler broadening) (eg., Pizzolato et al. 2003; Berger et al. 2010; Reiners & Basri 2010; Wright et al. 2011; McLean et al. 2012). This *activity-rotation relation* supports the hypothesis of a stellar magnetic dynamo that is *rotation-dependent*. The most successful dynamo model for solar-type stars, the $\alpha\Omega$ dynamo (Parker 1955), operates at the tachocline, the boundary between the radiative stellar core and the convective envelope. Shearing due to differential rotation helps drive the helical motion needed for dynamo action, so a rotation-dependence in the $\alpha\Omega$ dynamo is natural. Magnetic activity has also been connected with age, as more magnetically active stars are found to be systematically younger (Skumanich 1972; Hawley et al. 1996). Explanations for this association typically invoke rotational braking through magnetically-driven winds in the young, active stars (Skumanich 1972). These stars lose angular momentum to their winds, spinning down and reducing their magnetic activity over time (Skumanich 1972; West et al. 2008; Cranmer & Saar 2011).

Observations of rapidly-rotating stars show that magnetic activity reaches a so-called *saturation* regime, with $L_{\rm X}/L_{\rm bol} \approx 10^{-3}$ independent of rotation, for solar-type stars with rotation periods $P_{\rm rot} \lesssim 2$–3 days (e.g., Pizzolato et al. 2003; Berger et al. 2008a; Wright et al. 2011). No definitive explanation for this saturation exists, although possible sources include: a reduction in coronal volume/density from centrifugal stripping, a saturation in the surface filling factor of active regions, or a saturation in the dynamo efficiency itself (Vilhu 1984; Jardine & Unruh 1999; Stępień et al. 2001).

Evidence for *supersaturation*, a decrease in X-ray activity induced by extremely rapid rotation, was first found in G and K stars in clusters by Randich et al. (1996), a result which has been supported by Stępień et al. (2001) and Wright et al. (2011). The fastest rotators in these samples ($v \sin i \gtrsim 100$ km s^{-1}) were found to have X-ray activity below the saturated level ($L_{\rm X}/L_{\rm bol} \approx 10^{-3.5}$). Similar mechanisms to those suggested for saturation have been invoked to explain the magnetic supersaturation, particularly increased centrifugal stripping and a decrease in the efficiency of coronal heating. We provide a rigorous definition and discussion of supersaturation in §5.1.

1.2. *Magnetic Activity in the Ultracool Regime*

Magnetic field generation in the standard magnetic dynamo model relies on differential rotation in the radiative-convective boundary, and it is therefore expected that the $\alpha\Omega$ dynamo cannot be responsible for the magnetic fields of stars that are fully convective (dwarfs with spectral types $\gtrsim$ M3, or masses $\lesssim 0.35 M_\odot$, Chabrier & Baraffe 1997). Due to the inoperation of the $\alpha\Omega$ dynamo, it was originally anticipated that very-low-mass stars and brown dwarfs would not show observable magnetic activity. Indeed, measurements hint that X-ray and Hα activity decrease significantly in *ultracool dwarfs* (UCDs), defined here as those stars and brown dwarfs with spectral types M6.5 or later (e.g., Gizis et al. 2000; Mohanty & Basri 2003; West et al. 2004). However, the first detection of radio emission from a brown dwarf by Berger et al. (2001) affirmed that UCDs do, in fact, exhibit magnetic activity, and further work (Berger et al. 2010) found evidence for substantial radio activity *increase* relative to bolometric luminosity in UCDs, clearly showing that UCD magnetic activity can be quite strong.

The available observational data paints a complicated picture of magnetic activity in UCDs. X-ray and Hα emission in early-and-mid M dwarfs still follow rotation-activity relations similar to those observed in solar-type stars. Magnetic activity is found to reach saturation levels in some early-and-mid M dwarfs (Delfosse et al. 1998; Mohanty & Basri 2003) and there are hints of supersaturation in rapidly-rotating stars later than M7 (Berger et al. 2008a; McLean et al. 2012). No major changes in these activity-rotation relations are apparent at the theoretical transition into full-convection. Yet the lack of any saturation turn-off in radio emission suggests a breakdown in the X-ray/radio relation in the ultracool regime (Berger et al. 2008a; Stelzer et al. 2012; Williams et al. in prep.), hinting that either X-ray or radio emissions (or both) may no longer trivially trace the stellar magnetic fields.

Direct measurements of magnetic fields have provided some insight into the magnetic properties of fully-convective stars. The averaged magnetic field intensity of mid-M dwarfs increases with rotation, reaching saturated values around 2 kG, similar to spectral types earlier than the convective transition (Reiners & Basri 2010). The only significant change in stellar magnetism across the convective boundary is the proportion of field residing in large-scale components. Zeeman-Doppler imaging (ZDI) of early-M dwarfs suggests that the magnetic fields of partially-convective stars are dominated by the high-order multipolar components (i.e. tangled small-scale fields, Donati et al. 2008). On the contrary, spectropolarimetry of mid-M dwarfs by Morin et al. (2008) showed that, past the theoretical transition to full-convection, magnetic fields show a significant large-scale (dipolar or quadrupolar) component, despite no systematic change in overall magnetic field strength, a result which was confirmed by Reiners & Basri (2009). These direct measurements are, however, still limited to low rotational velocities — a significant restriction given that UCDs are systematically faster rotators (Mohanty & Basri 2003; Reiners & Basri 2010).

Theoretical modeling of UCD dynamos is faced with many problems, not the least of which include the complicated observational constraints. Early modeling attempts failed to reproduce the large-scale fields generated by these convective objects (Durney et al. 1993). While more recent MHD simulations have succeeded in reproducing fully-convective magnetic activity through α^2 or $\alpha^2\Omega$ dynamos, many problems exist with matching the observed field topologies (α^2: Küker & Rüdiger 1999; Chabrier & Küker 2006) or simulating high enough rotational velocities to probe observed activity-rotation

relations (Browning 2008).

Many intersecting issues therefore complicate the task of understanding the magnetic properties of ultracool dwarfs. Because they are systematically more rapid rotators, they could potentially represent the short-period end of the same activity-rotation relation found in solar-type stars, perhaps yielding clues as to the nature of supersaturation. Meanwhile, the transition to full-convection suggests that a separate dynamo mechanism must operate for UCDs, yet stars with spectral types as late as M7 still show rotational saturation identical to earlier types. Coronal and chromospheric activity has been observed to systematically decrease beyond M7 (Mohanty & Basri 2003; Reiners & Basri 2008; Berger et al. 2010), but whether this is due to the combination of faster rotation and supersaturation or simply the cool temperatures of UCDs is unclear. As suggested by Mohanty et al. (2002), coronal and chromospheric emissions may be suppressed by the decoupling of increasingly neutral UCD atmospheres from any magnetic fields present, making these activity indicators poor tracers of the underlying dynamo. Pursuit of these many unusual properties of UCDs may help overcome the theoretical challenges to understanding magnetism in fully convective stars.

In this paper, we investigate the X-ray activity-rotation relation in ultracool dwarfs, assembling a comprehensive sample of UCDs with X-ray and rotation measurements. This sample (presented in full in Table 6) makes use of new X-ray measurements, unpublished observations from the *Chandra* catalog, and a thorough search of the literature. This sample allows us to place unprecedented constraints on UCD X-ray activity properties and their dependence on various stellar parameters.

We proceed by describing our sample of UCDs, including the newly obtained X-ray measurements and the collection of various stellar parameters from the literature (§2). We also reference a large selection of early-type stars from the literature. We then describe the analysis of three unpublished observations found in the *Chandra* archives, including a discussion on flaring activity (§3). We then present an analysis of the activity-rotation relation in the UCD sample and examine correlations between activity and various rotation parameters (§4). We discuss several mechanisms which have been suggested to explain supersaturation, comparing their predictions to the observed relations in UCDs (§5). Finally, we summarize our results and conclusions (§6).

2. OBSERVATIONS

2.1. *Newly Observed UCDs*

The eight newly-observed objects included in our sample of active UCDs were observed in both X-ray and radio. We selected candidate objects by searching the database of dwarfarchives.org for nearby UCDs (spectral type M6.5 or later) without previous *Chandra* measurements and with available $v \sin i$ values, to allow for analysis of activity with respect to rotation. Candidates also have $\delta > -30°$, which allows VLA radio follow-up to be performed. Table 1 shows the major characteristics of the newly-observed UCDs, including the references from which the relevant values were gathered. X-ray observations were performed with *Chandra*. Details of the observations, as well as a more detailed discussion of the properties of each target, will be presented in Williams et al. (in prep.), but the key parameters are summarized in Tables 2 and 3.

We also identified observations of four UCDs in the *Chandra* Data Archive that have not been published. The details of the X-ray reductions of three of these objects (GJ 1245 AC, GJ 1245 B, and 2MUCD 10158) are presented in §3, while the reductions of the final star (LP 349–25 AB) will be included with the new observations in Williams et al. (in prep.).

2.2. *UCDs in the Literature*

Our UCD rotation-activity sample includes 23 UCDs collected from the literature. Objects included in the sample were required to have measurements of or upper limits to the X-ray luminosity and line-of-sight rotational velocity, as well as spectral types M6.5 or later. We believe our sample represents the complete collection of such objects available in the literature. Many previous rotation-activity studies have analyzed rotation in terms of photometrically derived rotation periods. We can estimate the rotation period using $v \sin i$ and a theoretical relation for stellar radius[3], although the unknown stellar inclination leads to a formal upper limit on period. Photometric rotation periods may exist in the literature for some of the UCDs in our sample, and an improvement upon the methods of this work would be to incorporate any available photometric rotation periods for our UCD sample.

Table 6 highlights the important parameters and X-ray properties of the objects in our sample, including both newly observed objects and objects from the literature.

2.3. *Comparison Objects*

Our UCD sample was analyzed in comparison to several other catalogs of X-ray active stars. James et al. 2000 studied a small sample of early-M dwarfs (see their Table 2) and found marginal evidence for X-ray supersaturation in the fastest rotators. Pizzolato et al. 2003 studied primarily solar-type stars (see their Tables 1 and 2), examining the limiting rotation period for saturation and finding saturation to begin at slower rotation for lower stellar mass.

3. NEW X-RAY REDUCTIONS

We present analysis of three nearby ($d < 5$ pc) late-type objects that have unpublished observations available in the *Chandra Data Archive*. All three objects were originally observed using the *Chandra*/ACIS-S3 backside-illuminated chip. We analyzed the data using *CIAO* version 4.5 (Fruscione et al. 2006) and the spectral analysis package *Sherpa* (Freeman et al. 2001). Analysis of the objects focused on the energy range 0.3–7 keV, where ACIS background is minimized[4]. An energy conversion factor of 1 count $= 4.5 \times 10^{-12}$ erg s^{-1} cm^{-2} (consistent with a $kT = 1$ keV Raymond-Smith plasma) is used when spectral reconstruction is not possible. We summarize the properties of these objects in Table 1,

[3] See §4.1 for the method used to approximate stellar radius.

[4] See http://cxc.harvard.edu/ciao/why/filter_energy.html for a discussion of recommended *Chandra* energy filters.

while Tables 2 and 3 show the X-ray observation details and results, respectively.

3.1. *2MUCD 10158*

2MUCD 10158 (also 2MASS J02550357-4700509 or DENIS-P J025503.3-470049) is an L8 brown dwarf (Reiners & Basri 2008) located at a distance of 4.97 pc (Costa et al. 2006, from parallax). The observation was performed in two parts (*Chandra* observation IDs 8903 and 10828), on 2 December 2008 (06:42:29–12:16:46 UT) and 4 December 2008 (18:57:10–22:15:40 UT), for a total exposure time of ∼28 ks.

We determined the position of 2MUCD 10158 at the times of observation using proper motion measurements gathered from the SIMBAD database. We extracted counts from a 2 arcsec radius aperture around the position of the source. A large (0.5 arcminute radius) circular aperture centered near the source but encompassing no point sources provided the background count rate. In the 0.3–7 keV range, only one photon was detected in the source region throughout both observations, compared to the expected background level of 0.7 counts per 28 ks in the same size region and energy range. Thus, the resulting upper limit was 4.3 counts (95% confidence, Kraft et al. 1991). Using the above energy conversion factor, the time-averaged flux limit is $F_{\rm X} < 6.9 \times 10^{-15}$ erg s^{-1} cm^{-2}. At a distance of 4.97 pc, we can thus constrain the persistent emission of 2MUCD 10158 as $L_{\rm X} \lesssim 2.1 \times 10^{24}$ erg s^{-1}, or $\log L_{\rm X}/L_{\rm bol} \lesssim -4.70$.[5]

3.2. *GJ 1245 System*

GJ 1245 ABC is a triple system at a distance of 4.54 pc. GJ 1245 A and B (M5.5 and M6.0, respectively, Henry et al. 2002) are separated by ∼7 arcseconds, while GJ 1245 A and C (M8.5, Law et al. 2008) form a tighter, 1 arcsecond binary. The *Chandra* observation of the system (observation ID 4476) occurred on 14 December 2003 (04:19:04–11:20:02 UT) with a total exposure time of ∼24 ks.

The wide binary (GJ 1245 A and B) is clearly resolved in the X-ray image (see Figure 1) but the tighter binary (GJ 1245 A and C) cannot be resolved. Hence, our analysis includes the combined X-ray emission from GJ 1245 A and C (hereafter GJ 1245 AC).

Due to the high count rate for each object (> 0.1 counts per second in some intervals), the effects of photon pileup were a concern. Pileup occurs when two or more photons impact on the same pixel during a frame and result in a single detection with measured energy equal to the sum of the individual photon energies. To estimate the pileup percentage during the observations, we used the *Chandra* Portable, Interactive Multi-Mission Simulator (*PIMMS*). For both objects, pileup was estimated at the ∼ 5% level, indicating approximately 5% of counts would have energies measured systematically too high. In order to understand and eliminate the effects of pileup, we analyzed the objects using both a circular aperture and an annulus centered on the source position, removing the center-most pixels where the count rate and likelihood of pile-up were greatest. Following estimations of pile-up fractions, we analyzed each object for indications of variability (i.e. flaring) and fit a spectral model to the binned data, yielding an estimate of and uncertainty on the X-ray flux from the object. Analysis where the annulus was used resulted in a loss of significant signal, but both sources were bright enough that we still retained a strong detection and spectrum.

[5] See §4.1 for the calculation of $L_{\rm bol}$.

3.2.1. *GJ 1245 AC*

The circular aperture (of radius 2 arcseconds) centered on the position of GJ 1245 A collected a total of 1607 counts between 0.3–7.0 keV, while the annulus (of inner radius 0.5 arcseconds and outer radius 2.25 arcseconds) yielded 407 counts in the same band. We performed variability analysis on the source using the method of Bayesian Blocks (Scargle et al. 2013). In this analysis, the X-ray count rate is modeled as piecewise constant over a variable number of bins, with the model complexity being controlled by a downward-sloping prior on the number of bins. The procedure combines an iterative approach with a Monte-Carlo derived parametrization of the prior to set the probability of false detection of an extraneous block at 2%. We present the results of this analysis in Figure 2, along with the light curve for GJ 1245 AC (binned every 200 seconds).

The analysis of the counts in the circular aperture divided the data into two bins, with a minor drop (≈ 30%) in emission in the second half of the observation. Although the difference in count rates is statistically significant in the Bayesian formalism, the long duration and low amplitude of the variability is not consistent with flaring behavior. We thus adopt the mean flux as a quiescent value. We additionally performed a Gregory-Loredo test (Gregory & Loredo 1992), which computes the likelihood of the measured light curve being consistent with a constant source. The Gregory-Loredo analysis yielded a variability index of 8, indicating the source is variable. Performing the same variability analysis on the counts captured in the annulus region yielded similar results suggesting long duration, low amplitude variability.

We extracted the X-ray spectrum from the annulus region, as even a small pile-up contamination (with systematically harder photons) could change the spectral fit significantly. We subtracted the background emission (using a large-radius aperture, centered nearby but encompassing no point sources) and evaluated the PSF coverage fraction of our extraction region. We used *Sherpa* to fit the source spectrum to a one-temperature Raymond-Smith plasma model, using a Monte-Carlo sampling method to find the best fit parameters. The source spectrum and resulting fit are shown in Figure 3.

Using the model spectrum, we generated a distribution of source flux values, in the range 0.3–7 keV. The model flux is $F_{\rm X} = (2.7^{+0.6}_{-0.5}) \times 10^{-13}$ erg s^{-1} cm^{-2}. At 4.54 pc, this places the mean X-ray luminosity of GJ 1245 AC at $L_{\rm X} = 6.7 \times 10^{26}$ erg s^{-1}, or $\log L_{\rm X}/L_{\rm bol} = -4.06$.

3.2.2. *GJ 1245 B*

Using a 2 arcsecond radius aperture, we measured 1072 counts from the source in the range 0.3–7 keV. The annulus (inner and outer radii 0.5 and 2.25 arcseconds, respectively) centered on the source position collected 154 counts in the same band. We performed identical variability analysis to that performed for GJ 1245 AC. For

Table 1
Properties of archived *Chandra* objects and newly-observed targets

Name	2MASS Identifier	SpT	Distance	$v \sin i$	References				
					P	M	S	D	V
			(pc)	(km s^{-1})					
Stars from *Chandra* archive									
GJ 1245 A	19535443+4424541 A	M5.5	4.55 ± 0.02	23 ± 2	1	18[a]	16	17	6
B	19535508+4424550	M6.0	4.55 ± 0.02	7 ± 2			16	17	6
C	19535443+4424541 C	M8.5	4.55 ± 0.02				16	17	
2MUCD 10158	02550357−4700509	L8	5.0 ± 0.1	67 ± 13	20		15	21	14
LP 349–25 A	00275592+2219328 A	M8	10.3 ± 1.7	55 ± 2	1	10	10	11	8
B	B	M9	10.3 ± 1.7	83 ± 3			10	11	8
New *Chandra* observations — see Williams et al. (in prep.)									
LHS 292[b]	10481258−1120082	M6.5	4.54 ± 0.07	<3	1		2	3	4
LHS 523	22285440−1325178	M6.5	$11.3 \pm^{0.7}_{0.6}$	~ 7.0	1		5	3	6
LHS 2397a A	11214924−1313084 A	M8	$14.3 \pm^{0.5}_{0.4}$	15 ± 1	1	7	7	3	8
B	B	L7.5	$14.3 \pm^{0.5}_{0.4}$	11 ± 3			7	3	8
LHS 3406	18432213+4040209	M8	14.1 ± 0.2	5 ± 3.2	1		9	3	4
LP 647–13	01095117−0343264	M9	11.1 ± 0.7	13 ± 2	12		9	9	4
LP 851–346	11554286−2224586	M7.5	9.7 ± 1.2	33 ± 3	1		13	13	4
NLTT 33370 AB	13142039+1320011	M7	16.4 ± 0.7	45 ± 5	12	22	23	23	24
NLTT 40026	15210103+5053230	M7.5	16.1 ± 1.6	40 ± 4	12		9	9	4

References. — Indicators are: P, discovery of substantial proper motion; M, discovery of multiplicity; S, spectral type; D, distance; V, $v \sin i$. [1] Luyten (1976), [2] Henry et al. (1994), [3] van Altena et al. (1995), [4] Reiners & Basri (2010), [5] Kirkpatrick et al. (1991), [6] Mohanty & Basri (2003), [7] Freed et al. (2003), [8] Konopacky et al. (2012), [9] Cruz et al. (2003), [10] Forveille et al. (2005), [11] Cruz et al. (2007), [12] Luyten (1979), [13] Crifo et al. (2005), [14] Reiners & Basri (2008), [15] Kirkpatrick et al. (2008), [16] Henry et al. (2002), [17] Jenkins et al. (2009), [18] Law et al. (2008), [19] Harrington & Dahn (1984), [20] Deacon et al. (2005), [21] Costa et al. (2006), [22] Law et al. (2006), [23] Lépine et al. (2009), [24] McLean et al. (2011)

[a] Discovery of GJ 1245 C
[b] Possible binary; see Guenther & Wuchterl (2003).

Table 2
X-ray observation details of archived *Chandra* objects and new *Chandra* observations

Name	ObsID	Observation Date		Integ. Time	Raw Counts
		Gregorian	MJD[TT]	(s)	
Stars from *Chandra* archive					
GJ 1245 AC	4476	2003 Dec 14	52987.18	23785	1607[a]
GJ 1245 B	4476	2003 Dec 14	52987.18	23785	1072[a]
2MUCD 10158[b]	8903	2008 Dec 02	54802.28	17993	0
	10828	2008 Dec 04	54804.79	9914	1
LP 349–25 AB	9925	2009 Sep 15	55089.28	37197	57
New *Chandra* observations — see Williams et al. (in prep.)					
LHS 292	13603	2011 Dec 14	55909.56	10620	48
LHS 523	13604	2012 Dec 08	56269.18	19605	9
LHS 2397a AB	13606	2012 Nov 05	56236.01	19804	236
LHS 3406	13609	2012 Dec 05	56266.17	19804	66
LP 647–13	13605	2012 Oct 24	56224.21	19798	9
LP 851–346	13607	2012 Jul 09	56117.63	19800	40
NLTT 33370 AB	14530	2013 Apr 28	56410.01	35588	834
NLTT 40026	13608	2013 Feb 07	56330.68	18812	4

Note. — The observation MJD is the approximate midpoint of the on-source integration. *Integ. Time* is the on-source integration time. *Raw Counts* is the number of counts in the energy band analyzed (see Table 3) in a 2" radius aperture around the predicted source position after processing in the VFAINT background mode.

[a] The high count rate for this object suggests the effects of pileup may be significant. See §3.2 for details.
[b] 2MUCD 10158 was observed in two parts, for a total exposure time of 27908 seconds.

Table 3
Results of new *Chandra* X-ray analysis and observations

Name	State	Integ. Time (s)	Counts (in band)	$\log F_X$ erg s^{-1} cm^{-2}	Band (keV)
Stars from *Chandra* archive — see §3					
GJ 1245 AC	Mean	23785	1607	$-12.57 \pm ^{0.08}_{0.09}$	0.3 − 7.0
GJ 1245 B	Mean	23785	1072	$-12.6 \pm ^{0.17}_{0.20}$	0.3 − 7.0
	Quiescent	21117	789	$-13.0 \pm ^{0.18}_{0.21}$	0.3 − 7.0
	Flare	2668	283	$-12.2 \pm ^{0.16}_{0.21}$	0.3 − 7.0
2MUCD 10158	Mean	27908	1	< -15.2	0.3 − 7.0
LP 349–25 AB[b]	Mean	37197	57	-14.2 ± 0.1	0.3 − 2.0
	Quiescent	8994	4	-14.7 ± 0.2	0.3 − 2.0
	Flare	28202	53	-14.1 ± 0.1	0.3 − 2.0
New *Chandra* observations — see Williams et al. (in prep.)					
LHS 292	Mean	10620	48	-13.7 ± 0.1	0.3 − 2.0
LHS 523	Mean	19605	9	-14.7 ± 0.2	0.3 − 2.0
LHS 2397a AB	Mean	19804	236	$-13.22 \pm ^{0.05}_{0.06}$	0.3 − 2.0
LHS 3406	Mean	19804	66	-13.9 ± 0.1	0.3 − 2.0
	Quiescent	17342	43	-14.0 ± 0.1	0.3 − 2.0
	Flare	2462	23	$-13.4 \pm ^{0.1}_{0.2}$	0.3 − 2.0
LP 647–13	Mean	19798	9	-14.7 ± 0.2	0.3 − 2.0
LP 851–346	Mean	19800	40	-14.1 ± 0.1	0.3 − 2.0
	Quiescent	18126	23	$-14.3 \pm ^{0.1}_{0.2}$	0.3 − 2.0
	Flare	1675	17	$-13.4 \pm ^{0.1}_{0.2}$	0.3 − 2.0
NLTT 33370 AB	Mean	35588	834	-12.92 ± 0.04	0.3 − 2.0
	Quiescent	35325	799	-12.94 ± 0.04	0.3 − 2.0
	Flare	263	35	-12.2 ± 0.1	0.3 − 2.0
NLTT 40026	Mean	18812	4	$-15.0 \pm ^{0.2}_{0.3}$	0.3 − 2.0

[a] The data reduction and analysis of LP 349–25 AB will be presented alongside the new observations in Williams et al. (in prep.).

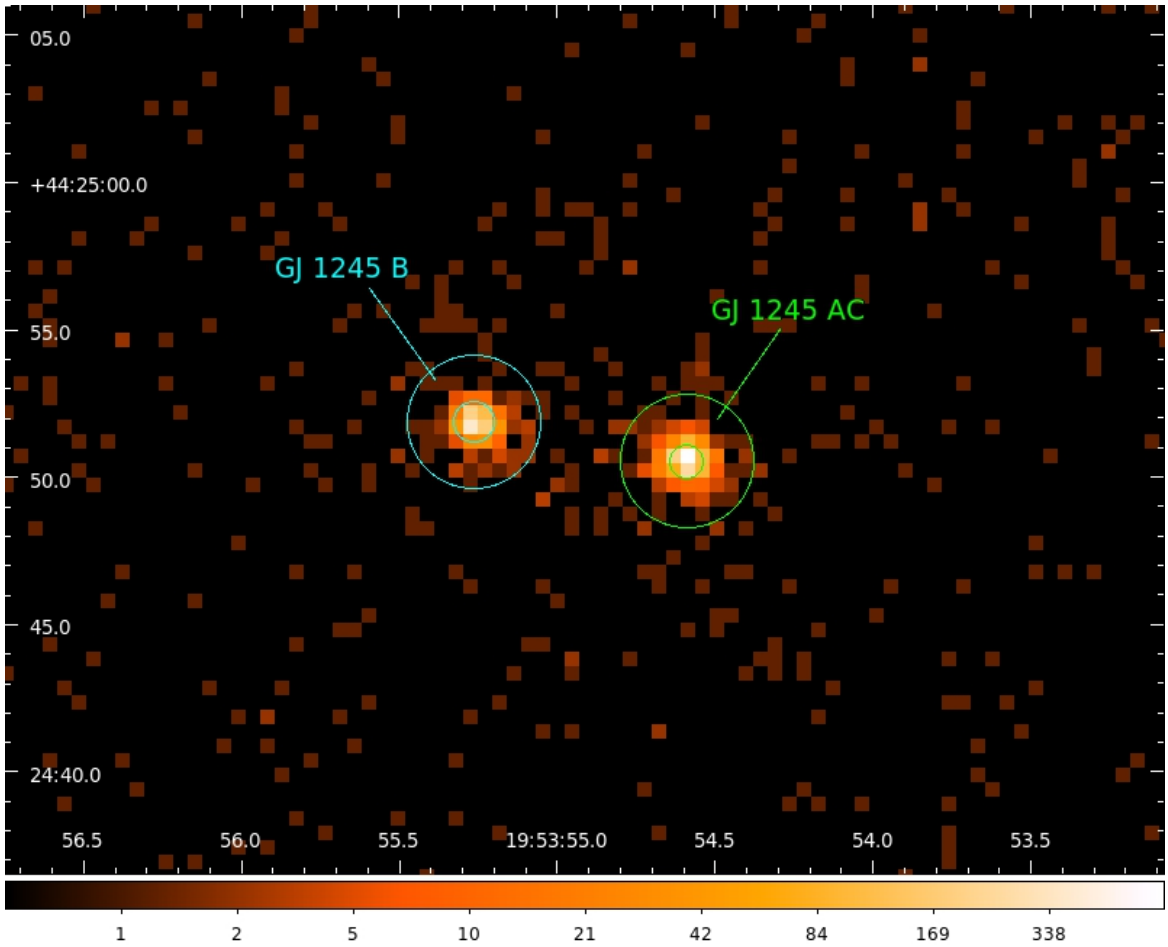

Figure 1. *Chandra* image of the GJ 1245 system. Shown is the clear X-ray detection of GJ 1245 B and the unresolved pair of GJ 1245 A and GJ 1245 C. The annulus around each object represents the area from which counts were extracted to avoid pileup in the central pixels (see §3.2.1). A colorbar below indicates the scale. Orientation is such that North is up and East is left.

GJ 1245 B, the Gregory-Loredo variability index was 10, indicating more significant variation in the source emission than for GJ 1245 AC. Furthermore, Bayesian Block analysis (prior parameter p0=0.02) on counts from the circular aperture region identified six significantly distinct regimes of emission. Most notably, we identify a large flare — lasting ≈ 0.75 hours — during which the count rate was 2.4 times higher than the average throughout the observation and 6.0 times higher than during the least active period. A smaller flare — lasting ≈ 0.41 hours and with count rate 3.4 times higher than the observed minimum — is also observed. The eye may be able to identify a third flare, particularly from the pattern of residuals, between the smaller and larger flare. A different approach to modeling the time-series variability (such as a piece-wise linear or exponential series, as mentioned in Scargle et al. (2013)) would likely have greater success at modeling the more complicated details of flaring. However, for our purposes, the piece-wise constant model was sufficient to identify the most statistically significant periods of overall emission. Variability analysis on the counts from the annulus region detected a strong increase in emission during the last half of the observation (with count rate 1.7× higher than average), but was unable to resolve the short duration of the strongest flare from the subsequent decline.

PIMMS predicted pileup to be a significant factor ($\sim$ 5%) on average throughout the observation of GJ 1245 B, with very high pileup fraction ($\sim$ 9%) during the strongest flaring period. Hence, we used the annulus region to extract the spectrum of GJ 1245 B from only the outer portions of the PSF, avoiding the inner pixels with high pileup fractions, identical to the procedure used for GJ 1245 AC. The source spectrum and a one-temperature Raymond-Smith model, as above, are shown in Figure 3.

Sampling from the model spectrum yielded an estimated flux $F_{\rm X} = (2.4^{+1.1}_{-0.9}) \times 10^{-13}$ erg s^{-1} cm^{-2} in the 0.3–7.0 keV band. Using the ratio of the flaring count rate to average, the flux during the large flare can be approximated as $F_{\rm X,f} \approx 5.8 \times 10^{-13}$ erg s^{-1} cm^{-2}, while the quiescent flux (using the count rate during the least active period identified in the Bayesian Blocks analysis) is $F_{\rm X,q} \approx 9.7 \times 10^{-14}$ erg s^{-1} cm^{-2}. At 4.54 pc, we measure GJ 1245 B to have a mean X-ray luminosity of $L_{\rm X} = 6.0 \times 10^{26}$ erg s^{-1}. The mean X-ray activity ratio is $\log(L_{\rm X}/L_{\rm bol}) = -3.89$, while the flaring and quiescent activity ratios are $\log(L_{\rm X,f}/L_{\rm bol}) = -3.52$ and $\log(L_{\rm X,q}/L_{\rm bol}) = -4.30$.

3.2.3. *Did ROSAT observe GJ 1245 during a flare?*

Previous X-ray observations of the GJ 1245 system were performed by the *ROSAT* All-Sky Survey (RASS), with follow-up on the *ROSAT* High Resolution Imager (HRI). The resolution of system into its separate compo-

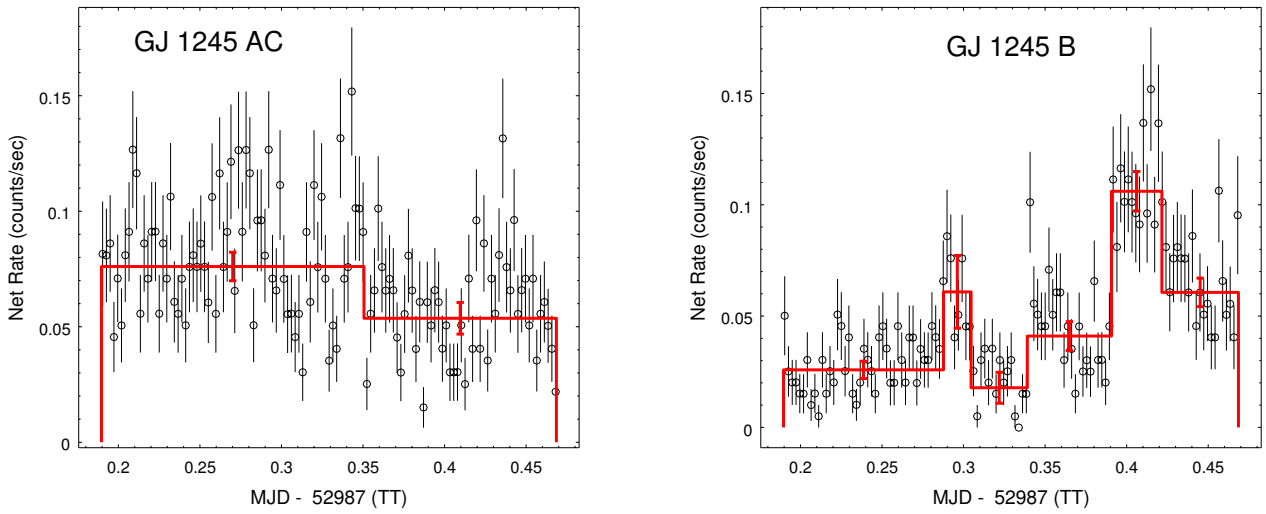

Figure 2. Binned light curves (200 seconds) for GJ 1245 AC and B, in the energy range 0.3–7 keV. Counts are extracted from a two arcsecond radius aperture around each source. Shown in red are piecewise constant histograms representing the statistically significant changes in mean count rate, produced using Bayesian Block variability analysis (see §3.2.1). *Left:* GJ 1245 AC — Bayesian Block analysis finds only two statistically significant regimes of emission, both of long duration, indicating no evidence for short-term flaring activity. Note the count rate consistently near 0.1 counts per second, suggesting high likelihood for pileup. *Right:* GJ 1245 B — A clearly variable signal is supported by Bayesian Block analysis, which finds six separate regimes of emission. Most notable is the detection of an extremely high period of emission around MJD 52987.40, lasting approximately 44.5 minutes at peak, which we interpret as a strong flare. A smaller flare is possibly found around MJD 52987.28. The lowest count rate is between MJD 52987.30 and 52987.34, which we adopt as the quiescent emission period.

nents (namely, GJ 1245 AC and GJ 1245 B) by RASS is at issue, however. Law et al. (2008) matched the position of GJ 1245 A to an X-ray source from RASS, finding the X-ray luminosity of GJ 1245 A to be $L_{\rm X,A} = 2.94 \times 10^{27}$ erg s^{-1}, a factor of 4 times higher than that measured by *Chandra* (§3.2.1). Yet the angular resolution of RASS was only $\approx$ 5–10 arcminutes (Voges et al. 1999) and clearly was insufficient to resolve the 7 arcsecond separation between GJ 1245 A and B. Schmitt & Liefke (2004) correctly identify the same X-ray source as the combined emission from GJ 1245 A, B, and C. Our *Chandra* analysis places the combined, mean X-ray luminosity of the system (converted to the same 0.1–2.4 keV band as *ROSAT*) at $L_{\rm X,AC} + L_{\rm X,B} = 1.43 \times 10^{27}$ erg s^{-1}, still less than half of the measured *ROSAT* luminosity.

We believe this is evidence that the RASS measurements managed to observe the GJ 1245 system during a strong flare. The RASS exposure time during the GJ 1245 system observation was 730 seconds (Schmitt & Liefke 2004), well shorter than the timescale of the strong flare observed on GJ 1245 B by *Chandra* ($\sim$ 2600 seconds). The estimated combined luminosity (in *ROSAT*'s 0.1–2.4 keV band) of GJ 1245 AC and B during GJ 1245 B's *Chandra*-observed flare was $L_{\rm X,AC} + L_{\rm X,B,Fl.} \approx 2.4 \times 10^{27}$ erg s^{-1}, closer to the value recorded by RASS. Later *ROSAT* measurements using the HRI find $L_{\rm X,ABC} = 1.55 \times 10^{27}$ erg s^{-1} over an integration time of 2849 seconds (Schmitt & Liefke 2004), in better agreement with the average combined luminosity measured by *Chandra*. As typical X-ray flaring factors (the ratio of flaring to quiescent luminosity) for our UCD sample range from 2 to 10 or more, it would not take an unusually large flare to account for the $\sim$ 2 times overluminosity of the GJ 1245 system observed by RASS.

4. X-RAY ACTIVITY TRENDS

4.1. *Calculating Stellar Properties*

Many X-ray observations are sensitive to different energy regimes; for consistency we normalized all X-ray fluxes and luminosities to a common band of 0.2–2.0 keV. We used *PIMMS* to approximate the conversion ratio between flux in a given energy band and the 0.2–2.0 keV regime, the results of which are shown in Table 4. We assumed a Raymond-Smith plasma spectral model, and evaluated the conversion factor for a range of different plasma temperatures. The chosen conversion factors represent an approximate median for several temperatures in the range $kT = 0.4$–1.0 keV and is stable to within 5% for temperatures within this range.

Stellar X-ray activity is commonly analyzed in terms of the ratio of X-ray to bolometric luminosity, thus indicating what fraction of the total radiative energy is emitted in X-rays. Hereafter, we will designate *X-ray activity* to mean the ratio of X-ray luminosity ($L_{\rm X}$, in 0.2–2.0 keV band) to the bolometric luminosity ($L_{\rm bol}$). To approximate bolometric luminosity for our sample of UCDs, we applied a bolometric correction[6] to the absolute magnitude of each star. For M dwarfs, we took the average of the bolometric luminosity calculated using J and K band magnitudes:

$$\mathrm{BC}_K = 2.43 + 0.0895 \times (\mathrm{SP})$$

and

$$\mathrm{BC}_J = 1.53 + 0.148 \times (\mathrm{SP}) - 0.0105 \times (\mathrm{SP})^2$$

[6] $L_{\rm bol} = \mathrm{L}_{\odot} \times 10^{0.4 \times (M_{\odot,bol} - M_* - BC)}$, where M_* is the absolute magnitude of the star in a given band, BC is the applied bolometric correction for that band, and $M_{\odot,bol}$ is the bolometric absolute magnitude of the Sun (taken to be 4.7554).

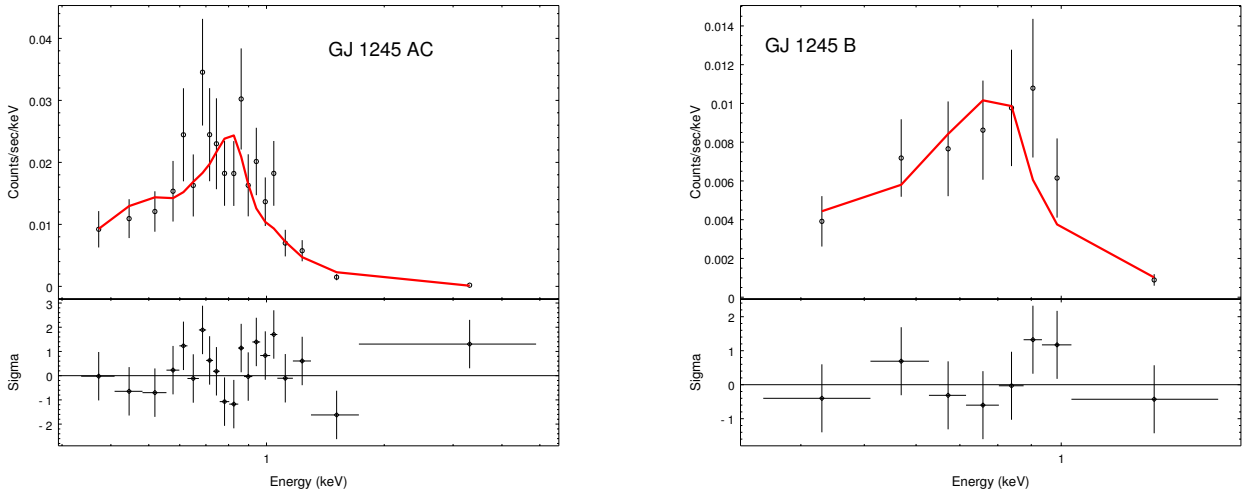

Figure 3. Measured spectra for GJ 1245 AC and B. Counts are extracted from annuli with inner and outer radii 0.5 and 2.25 arcseconds, respectively, to minimize the effect of pileup from the central pixels. Shown in red is the best-fit spectral fit, using a one-temperature Raymond-Smith (RS) plasma model. Residuals from the fit are shown below each spectrum. *Left:* GJ 1245 AC — Best-fit model is a RS plasma with $kT = 0.473$ keV and metallicity $= 0.021\times$ solar. The fit statistics are $\chi^2_R = 1.21$ for 17 DOF. The model flux distribution is $F_{\rm X} = (2.72^{+0.6}_{-0.5}) \times 10^{-13}$ erg s^{-1} cm^{-2} (0.3–7 keV). Using a two-temperature RS model does not significantly improve the fit. *Right:* GJ 1245 B — Best-fit model is a Raymond-Smith plasma with $kT = 0.370$ keV and metallicity $= 0.039\times$ solar. The fit statistics are $\chi^2_R = 0.88$ for 5 DOF. The model flux distribution is $F_{\rm X} = (2.4^{+1.1}_{-0.9}) \times 10^{-13}$ erg s^{-1} cm^{-2} (0.3–7 keV).

Table 4
X-Ray Energy Band Conversion Factors

Original Band keV	Conversion Factor
0.2–2.0	1.00
0.1–2.4	0.84
0.1–10	0.80
0.2–8.0	0.95
0.3–0.8	1.53
0.3–2.0	1.10
0.3–7.0	1.05
0.3–8.0	1.05
0.5–8.0	1.20

Note. — Energy Band Conversion factors, used to convert flux from a given X-ray energy band to a standard 0.2–2.0 keV band. Flux in the 0.2–2.0 keV band is approximated by flux in the original band multiplied by the listed conversion factor. Conversion factors were calculated using *PIMMS*, asssuming a Raymond-Smith spectral shape and a plasma temperature in the range $kT = 0.4$–1.0 keV.

with SP = 0 (5) for spectral type M0 (M5) (Wilking et al. 1999). For L dwarfs, we use only the K-band correction:

$$\begin{aligned} {\rm BC}_K &= 2.37 + 0.075 \times ({\rm SP}) \quad 10 \le {\rm SP} \le 14 \\ &= 4.47 - 0.075 \times ({\rm SP}) \quad 14 \le {\rm SP} \le 19 \end{aligned}$$

for the same definition of SP as above (SP = 10 for L0) (Nakajima et al. 2004). The results of this analysis for the UCD sample are presented in Table 6.

Rotation periods are derived from $v \sin i$ and stellar radius. We approximated radii using the empirical mass-luminosity relation of Delfosse et al. (2000) in conjunction with the theoretically derived mass-radius relation of Baraffe et al. (1998). This method is consistent with Reiners & Basri (2010), Muirhead et al. (2012), and McLean et al. (2012), among others. Stellar radius is fairly constant in the UCD regime, and thus any uncertainties in the rotational period are dominated by sources other than the mass-radius relation. However, we note that, due to the confounding inclination parameter, the rotational periods derived from $v \sin i$ are upper limits. Making the reasonable assumption of random inclinations, we predict that no significant bias should be introduced. The expected value of $\sin i$ given a rotation axis oriented randomly in space relative to the observer is simply $\frac{1}{2}$, and thus the period calculated using $v \sin i$ will be overestimated by only a factor of about 2 (0.3 dex). No X-ray selection effects are likely, as X-ray emission is expected to be mostly uniform.

Noyes et al. (1984) first suggested that the *Rossby number*, the ratio of the rotational period and the *convective turnover time* τ_c, may be a stronger predictor of magnetic activity than the rotational period alone, a proposition which has been supported by later work, such as Pizzolato et al. (2003) and Wright et al. (2011). We calculated the convective turnover time for our sample using the method of Reiners & Basri (2010) and Kiraga & Stępień (2007), yielding — in conjunction with the rotation period — an upper limit on the Rossby number, $Ro = \frac{P_{rot}}{\tau_c}$. The relations used are:

$$\begin{aligned} \tau_c({\rm days}) &= 61.7 - 44.7 \times m, & 0.82 \le m < 1.30 \\ &= 25, & 0.65 \le m < 0.82 \\ &= 86.9 - 94.3 \times m, & 0.10 \le m < 0.65 \\ &= 70, & m \le 0.10 \end{aligned}$$

for $m = \frac{M_*}{{\rm M}_\odot}$. We note, however, that the convective turnover time is ill-defined at these low masses, as τ_c may vary widely with location within the convective region

(the entire star, in spectral types M3 or later). τ_c is approximated constant (70 days) for spectral types later than ∼M7. The Rossby number is therefore essentially equivalent to the rotation period for almost all of our sample of UCDs.

Also calculated is the *corotation radius* — the radius at which the centripetal forces of corotation with the star are balanced by gravity — in units of the stellar radius:

$$R_{corot}/R_* = \left(\frac{GM_*P_{rot}^2}{4\pi^2 R_*^3}\right)^{1/3} \propto M_*^{1/3} P_{rot}^{2/3} R_*^{-1}\,.$$

The ratio of the corotation radius to the stellar radius is often used as a measure of the strength of centrifugal stripping effects in the corona (Jardine & Unruh 1999; James et al. 2000).

4.2. *UCD Activity Trends*

The X-ray activity of our ultra-cool dwarf sample is plotted against the rotation period, Rossby number, and corotation radius in Figure 4. Also included for comparison are the samples of Pizzolato et al. (2003) and James et al. (2000), which studied the X-ray activity-rotation relation in A–M6 and M0–M5 dwarfs, respectively.

Figure 4 clearly shows the pre-saturation and saturation regimes in stars earlier than type M3. All mid-M (M3–M6, shown in red) stars appear to be saturated. UCDs (shown in blue and green) are systematically faster rotators, in terms of both period and Rossby number, than earlier-type stars. Many of the UCDs show X-ray emission well below the saturation level of $L_X/L_{bol} \approx 10^{-3}$, with many UCDs (including late-M dwarfs) emitting at detectable levels as low as $L_X/L_{bol} \approx 10^{-5}$.

It is important to understand whether this decrease in X-ray activity is caused purely by faster rotation or is due to other stellar parameters, such as temperature, size, or age, that are correlated with rotation. To investigate, we analyzed the dependence of UCD X-ray activity on the rotational parameters $v \sin i$, P_{rot}, and Ro. We wished to isolate any rotational effects from the complicating influence of spectral type, as a purely temperature-dependent decrease in X-ray activity could cause a spurious correlation with rotation due to the loose correlation observed between spectral type and rotation velocity. To this end, we performed our analysis on both the full UCD sample and a subsample of UCDs in the narrow spectral type range M6.5–M9.5. This sub-sampling suppresses the influence of effective temperature on activity, as T_{eff} decreases by only ∼ 500K between M6.5 and M9.5 (Luhman et al. 2003). While later spectral types are more likely to be fast rotators (see Figure 5), $v \sin i$ is not strongly correlated with spectral type over the narrow spectral type range selected. Thus, any association between X-ray activity and rotation in this subsample is most likely due to rotation alone. Only quiescent emission states are analyzed, and known tight binaries are removed from the M6.5–M9.5 subsample, consistent with the analysis of Pizzolato et al. (2003). Konopacky et al. (2012) showed that, in some UCD binaries, $v \sin i$ can differ significantly (by up to 30 km s^{-1}) between components, and it cannot be determined from available data alone whether X-ray activity or rotational velocity are influenced by a blending of the components.

Several UCDs in our sample (particularly L dwarfs) were non-detections in X-ray. Data representing merely an upper or lower limit of a value are known as *censored* data. The field of *survival statistics* deals with recovering the most statistical information possible from data sets containing censoring. One extremely useful example is in fitting regressions to multidimensional data, as various survival techniques can utilize censored data points to provide some constraint on the fit parameters which classical regression methods would be unable to accomplish. Chapter 10 of Feigelson & Babu (2012) provides an excellent introduction to the statistics of censored data sets, with applications and examples for astronomy.

The R package *NADA* (Helsel 2005) provides a number of useful survival analysis methods. We fit regressions to the available UCD data using a Maximum Likelihood Estimator (MLE) method based upon an accelerated failure-time model[7]. One benefit of this method is it allows for automatic calculation of the likelihood ratio of the parametrized model to a model without dependence on rotation, yielding a statistical *p-value* which indicates the strength of the correlation. To estimate the uncertainty on the fit parameters, we performed a bootstrap analysis, running 10,000 iterations on the fit, sampling with replacement and calculating the MLE fit parameters for each sample. The distributions of fit parameters for all regressions are approximately normal, so the standard deviation of the distribution is adopted as the uncertainty of each fit parameter.

The results of the survival analysis regressions are shown in Table 5. Each regression finds that X-ray activity decreases with faster rotation in UCDs. The p-values of the regressions range between $p < 0.01$ and $p < 0.03$. Taken together, the regressions allow us to claim with reasonable certainty that there is a significant anticorrelation between rotation and activity. Figure 6 shows the L_X/L_{bol} vs. $v \sin i$ regressions derived for both the entire UCD sample and the subsample of M6.5–M9.5 dwarfs.

5. POSSIBLE CAUSES OF DECREASED X-RAY EMISSION IN UCDS

With our large sample of X-ray observed ultracool dwarfs with rotation measurements, we are able to place unprecedented constraints on the relationships between X-ray activity, rotation, and spectral type. All UCDs in this sample are observed to be fast rotators ($v \sin i > 3$ km s^{-1}), where activity-rotation relations for early-M stars would predict X-ray emission to be saturated near $L_X/L_{bol} \approx 10^{-3}$. Yet many UCDs show quiescent emission well below the saturated level, with detections as much as two orders of magnitude below saturation. All L-dwarfs (with the exception of one shallow non-detection) emit well below the saturation value, yet emission varies widely within spectral type for late-M dwarfs. While the early-M activity-rotation relation appears to break down in stars cooler than M6.5, temperature is most likely not the only factor influencing the decrease in activity, as evidenced by the anticorrelation between activity and rotation in the narrow spectral type subsample.

Our analysis in §4.2 found significant evidence for an

[7] Method *cenmle*

Table 5
X-ray Activity-Rotation Regression Parameters
$\log(Y) = a \times \log(X) + b$

Y	X	a	b	Prob.
		Full UCD sample		
L_X	$v \sin i$ (km s^{-1})	-1.6 ± 0.6	27.3 ± 0.7	p< 0.02
L_X/L_{bol}	$v \sin i$ (km s^{-1})	-1.1 ± 0.5	-3.3 ± 0.6	p< 0.02
L_X/L_{bol}	P_{rot} (days)	1.3 ± 0.5	-4.1 ± 0.3	p< 0.01
L_X/L_{bol}	Ro	1.3 ± 0.5	-1.7 ± 1.1	p< 0.01
		Subsample: M6.5–M9.5 dwarfs, no binaries		
L_X	$v \sin i$ (km s^{-1})	-1.6 ± 0.7	27.5 ± 0.9	p< 0.02
L_X/L_{bol}	$v \sin i$ (km s^{-1})	-1.2 ± 0.7	-3.2 ± 0.8	p< 0.03
L_X/L_{bol}	P_{rot} (days)	1.2 ± 0.7	-4.1 ± 0.3	p< 0.03
L_X/L_{bol}	Ro	1.3 ± 0.7	-1.8 ± 1.5	p< 0.03

Note. — Regression parameters derived using MLE method described in §4. The fit can also be expressed as $Y \propto X^a$. While significant scatter exists in the data, the likelihood analysis allows us to dismiss no correlation with rotation with at least 97% confidence. Interestingly, the fit for the entire UCD sample is consistent with the subsample of M6.5–M9.5. This indicates that, while later spectral types are systematically faster rotators, spectral type variations alone are not entirely responsible for the observed correlation; rotation has a significant influence on X-ray emission.

anticorrelation between X-ray activity and rotation in UCDs. This is found both in the total UCD sample and in a subsample of M6.5–M9.5 stars, where rotation is not strongly correlated with spectral type and temperature changes by less than $\sim 20\%$. We believe this to be the strongest evidence to date of a breakdown in the standard X-ray activity-rotation relation in UCDs. We now consider various possible explanations for this reduction in X-ray activity in UCDs, which we group into two broad groups. Explanations which argue for a *supersaturation* mechanism suggest a causal relation between rapid rotation and reduced activity levels, while *anticorrelation* implies the influence of an unknown, third stellar parameter which independently affects both rotation and activity and explains the observed trend.

5.1. *Supersaturation Mechanisms*

Many explanations for supersaturation of magnetic activity in ultra-fast rotators have been put forward. In solar-type (G/K) type stars where the rotationally-driven $\alpha\Omega$ dynamo is believed to generate magnetic activity, it has been suggested that supersaturation may be due to a decrease in dynamo efficiency with extremely fast rotation (Vilhu 1984; Randich 1998). The $\alpha\Omega$ dynamo is not believed to operate in fully-convective UCDs, and a turbulent dynamo is expected to have only a mild dependence on rotation (Durney et al. 1993). A rotationally-dependent α^2 dynamo, on the other hand, could presumably show supersaturation effects at high rotation, possibly explaining the decrease in coronal emission found here in ultra-rapid rotators. However, work by Berger et al. (2010) and McLean et al. (2012) shows that radio emission in some UCDs does not saturate or supersaturate with fast rotation, as coronal and chromospheric activity appear to. Instead, radio activity in stars as late as L4 increases with rotation to several orders of magnitude above the saturation level of solar-type stars, implying the continued operation of a magnetic dynamo.

Another proposed cause of supersaturation is centrifugal stripping of the coronal envelope (Jardine & Unruh 1999; James et al. 2000; Jardine 2004). This theory suggests that centrifugal forces in the outer coronae of rapidly rotating stars lead to an increase in coronal pressure and density, which increases the X-ray emissions coming from a given coronal volume. The volume of the emitting coronal regions will, however, be limited by the corotation radius. Jardine & Unruh (1999) argues that, in the moderate-rotation regime, the two effects will cancel, leading to X-ray saturation. At sufficiently rapid rotation periods, the coronal volume stripping is enough to reduce the overall X-ray emission, causing the observed supersaturation effect.

The point at which centrifugal stripping would result in supersaturation depends on the characteristic height of magnetic field loops in the corona. Wright et al. (2011) claims to find evidence for supersaturation (activity decrease from $L_X/L_{bol} \approx 10^{-3}$ to $\approx 10^{-3.5}$) in solar-type stars only at values of $R_{corot}/R_* \approx 2$–3, suggesting that the scale of major coronal features extends only to about $1R_*$ above the stellar surface. Yet, as shown in Figure 4, UCDs with suppressed X-ray emission in our sample have values of R_{corot}/R_* as high as 10 or more, in the same range as solar-type stars which show saturated emission. If centrifugal stripping is responsible for supersaturation in UCDs, the relative sizes of their coronal loops must be at least 5 times larger than even early M-dwarfs, in which Wright et al. (2011) finds no evidence for supersaturation down to $R_{corot}/R_* \lesssim 3$. Furthermore, the magnitude of the observed X-ray activity decrease (nearly two orders of magnitude) is much more significant than the "supersaturation" observed in solar-type stars and would suggest an incredible disturbance of the stellar coronae. We

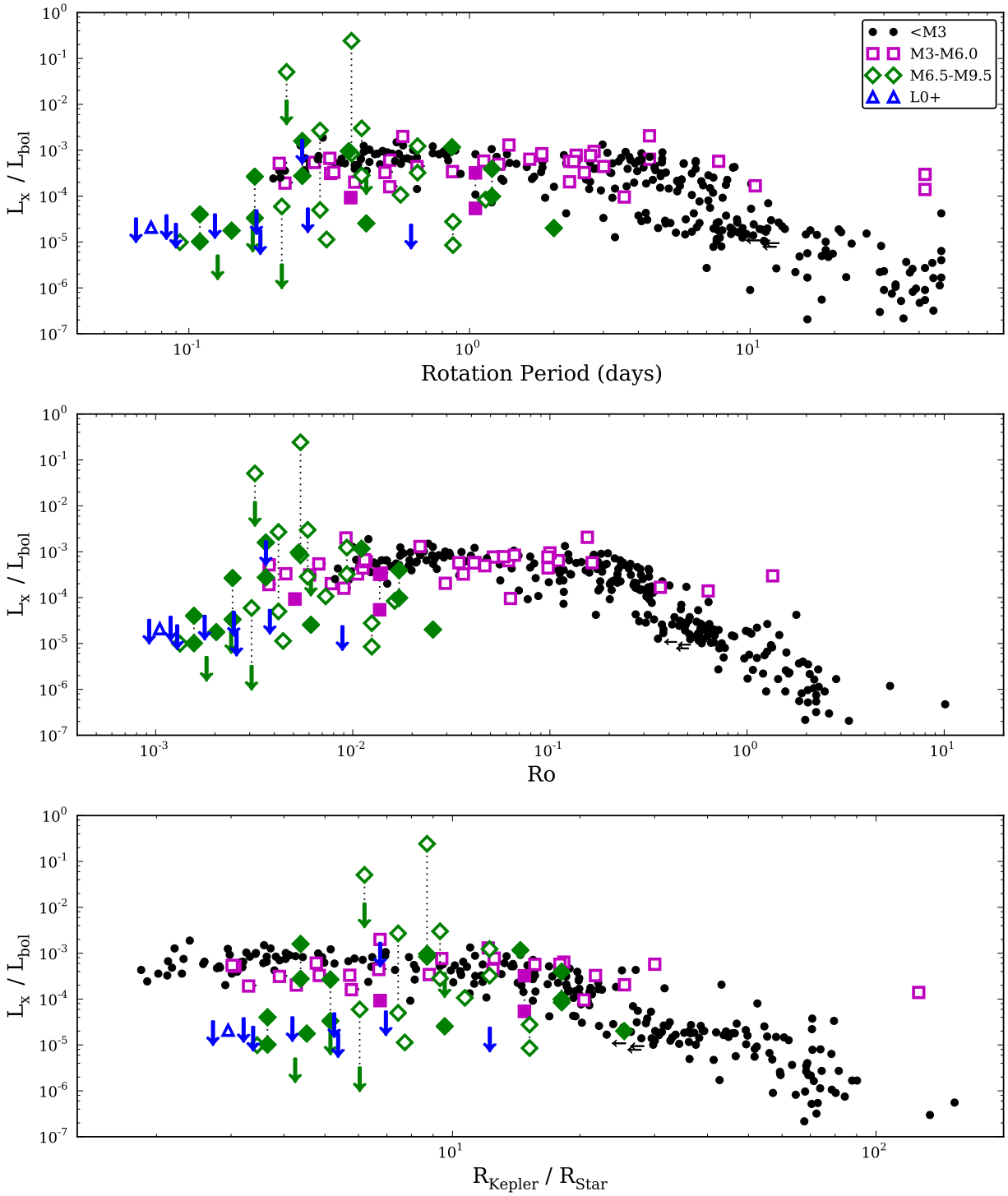

Figure 4. X-ray activity (0.2–2.0 keV) versus various rotation parameters, as calculated in §4. Plotted are all objects in our sample as well as objects from James et al. (2000) and Pizzolato et al. (2003). We note that all UCD rotation parameters are formally upper limits, due to unknown inclination in $v \sin i$. Points connected by a dotted line represent flaring and quiescent states for the same object. Spectral types are denoted by the following symbols: Black circles ($\leq$M2), Red squares (M3–M6), Green diamonds (M6.5–M9.5), Blue circles ($\geq$L0). Downward-facing arrows indicate X-ray non-detections. Solid symbols indicate new measurements presented in this work and in Williams et al. (in prep.). In all three images, the typical activity-rotation correlation at slower rotation values, the regime of X-ray saturation around $L_X/L_{bol} \sim 10^{-3}$, and a large population of rapid-rotators with activity well below the saturation level, are apparent. *Upper*: X-ray activity versus rotation period. *Middle*: X-ray activity versus Rossby Number, Ro = P_{rot}/τ_c, the ratio of the rotation period to the convective turnover time. *Lower*: X-ray activity versus Jardine & Unruh 1999's centrifugal stripping parameter. James et al. (2000) measurements are not included, because there is insufficient information to estimate the masses of the objects in that sample. Interestingly, the fastest-rotating UCDs have larger centrifugal stripping parameters than many of the slower-rotating solar-type stars. This suggests that centrifugal forces are not likely to be causing "supersaturation" in the UCDs. This is discussed further in §5.1.

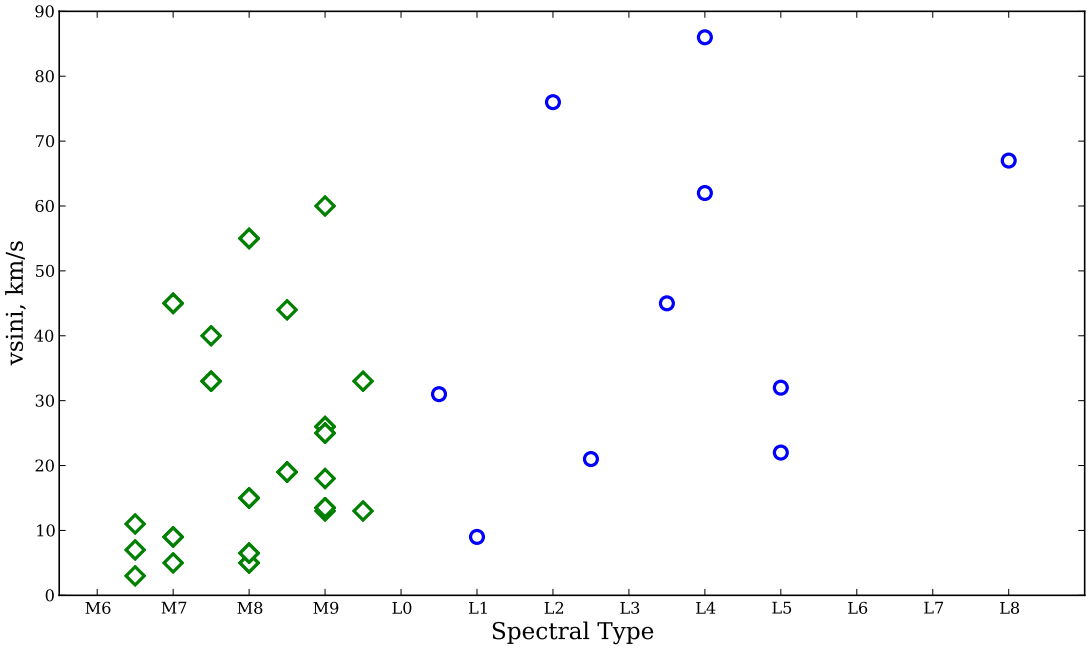

Figure 5. The line-of-sight component of rotational velocity for our UCD sample, as a function of spectral type. Blue symbols represent L-dwarfs and green symbols represent M-dwarfs. It can be seen that L-dwarfs are systematically faster rotators, in agreement with the findings of Reiners & Basri (2010). However no strong correlation with spectral type exists over the narrow spectral type regime M6.5–M9.5. Our analysis thus incorporates a subsample of UCDs in this range, in order to isolate the influence of spectral type (temperature) from purely rotational dependences.

therefore do not find it reasonable that centrifugal stripping is the only driving mechanism behind the decreased emissions found in UCDs. Another dramatic change in stellar properties must occur to explain why centrifugal stripping would affect UCDs at larger radii than solar-type stars.

5.2. *Sources of Anticorrelation*

Ultimately, the correlation between activity and rotation, while significant, does not demonstrate an causal connection between the two parameters. Although our analysis indicates a general trend towards lower activity with faster rotation, the existence of pairs of stars with similar spectral types and rotation velocities yet vastly different X-ray activity levels challenge the interpretation of direct supersaturation caused by rotation. For example, the M9 dwarfs LHS 2065 and 2MASS J10481463-3956062 ($v \sin i$ = 13.5 and 18 km s^{-1}, respectively) likely have similar masses, temperatures, and rotational velocities, yet differ by over an order of magnitude in X-ray activity ($L_{\rm X}/L_{\rm bol}$ = −3.55 and −4.95). The overall scatter in X-ray activity among rapid rotators is much larger in UCDs than in solar-type stars: for solar-type stars in the Pizzolato et al. (2003) sample with $P_{\rm rot} < 1$ day, the standard deviation in activity is $\sigma(\log L_{\rm X}/L_{\rm bol}) = 0.25$, while for UCDs in the same rotation range, $\sigma(\log L_{\rm X}/L_{\rm bol}) = 0.85$. We speculate that an unknown parameter, weakly correlated with both rotation and activity, may be responsible for the large scatter present in the activity-rotation relation.

X-ray activity reduction in UCDs has been suggested to be caused by a decrease in coronal heating efficiency, perhaps due to effects such as increased electron trapping (Berger et al. 2008a, 2010), which would reduce coronal emissions yet could still allow for strong radio activity. Other authors (e.g., Mohanty & Basri 2003; Reiners & Basri 2008; McLean et al. 2012) similarly suggest that the magnetic field may begin to decouple from the increasingly-neutral atmosphere as temperature decreases, reducing the efficiency of chromospheric and coronal heating by magnetic reconnection. While temperature effects may play some role in the evolution of activity levels with spectral type, it is difficult to understand how these mechanisms alone could explain the rotational dependence of X-ray activity found in the current sample of active UCDs, which is observed even in the M6.5–M9.5 subsample that isolates a population of similar temperatures and masses. Purely temperature-dependent arguments additionally cannot explain the widely varying X-ray activity among stars with similar spectral types.

Recent spectropolarimetry results show that the topology of stellar magnetic fields changes dramatically in the fully-convective regime. While partially-convective solar-type and early-M dwarfs show little evidence of large-scale magnetic fields, the field topologies of mid-M dwarfs demonstrate a substantial fraction of large-scale components. Using Zeeman-Doppler imaging (ZDI) techniques, Morin et al. (2008) mapped the large-scale magnetic fields of six fully-convective M3–M4.5 stars, finding in all cases strong, low-multipolar components of the magnetic field. Continuing this analysis into the spectral type range M5–M8 (including GJ 1245 B, VB 8, and VB 10 from our sample), Morin et al. (2010) found that late-M stars can exhibit either strong large-scale magnetic fields (similar to mid-M stars) or fields with weak large-scale components, dominated by small-scale fields (similar to solar-type stars). The strong-and-weak large-

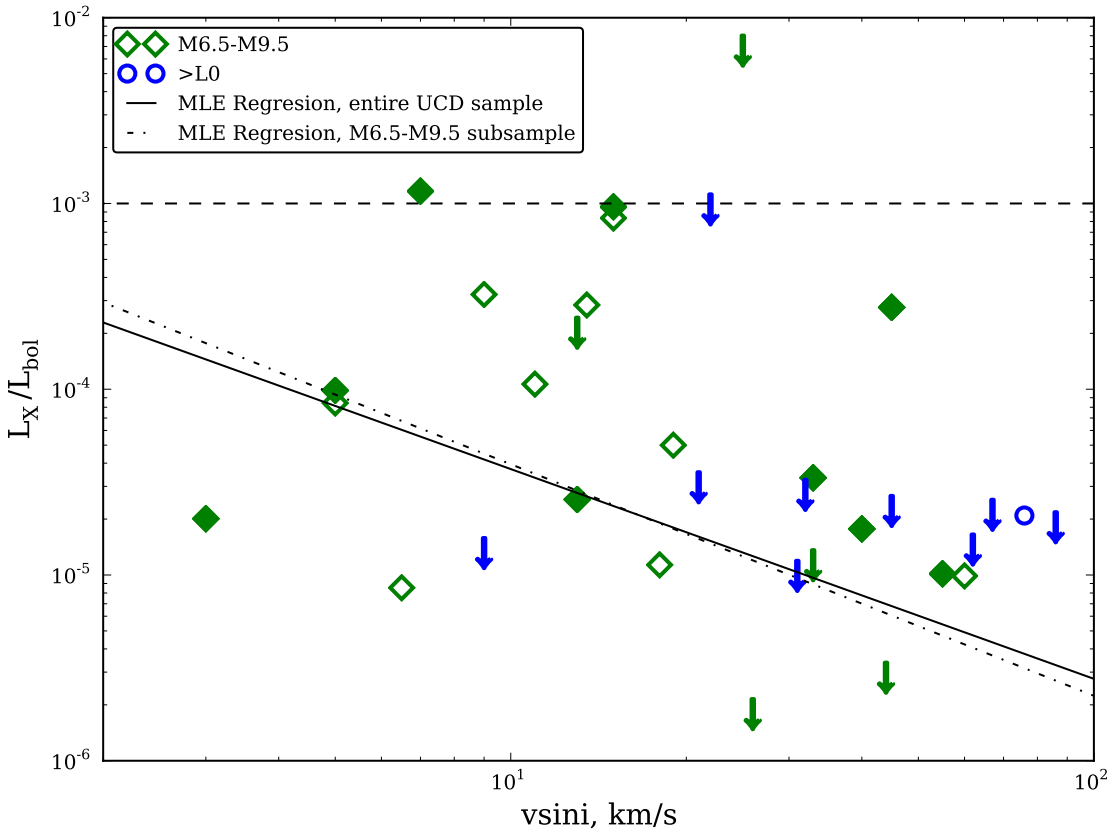

Figure 6. The activity-rotation relation for our sample of UCDs. The X-ray activity is shown converted to the 0.2–2.0 keV band. Symbols and colors are the same as in Figure 4. Although significant scatter exists in the data, a general trend towards lower activity with faster rotation is apparent. The regressions between L_X/L_{bol} and $v \sin i$ for both the full UCD sample and the M6.5–M9.5 subsample are shown, indicating an apparent anticorrelation between activity and rotation velocity.

scale fields showed no trivial dependence on mass or rotation, as *both topologies were observed in stars with similar masses and rotation periods.* Further theoretical work (Morin et al. 2011; Gastine et al. 2013) suggests that two separate dynamo regimes (a so-called *strong-field* regime and a *weak-field* regime) could be mutually stable in low-mass stars.

The large-scale magnetic field strengths for the few objects studied in Morin et al. (2010) correlate with rotation and spectral-type in a remarkably similar fashion to the observed X-ray activity/rotation/spectral-type relations in M-dwarfs (see their Figure 16). Mid-M dwarfs (mostly rapid rotators with Ro $< 10^{-1}$) have "saturated" large-scale field strengths ($\sim$ 600 G) independant of rotation. Late-M dwarfs (Ro $\lesssim 10^{-2}$) show large scatter in their large-scale strengths, with some occupying the saturated branch and others falling as much as an order of magnitude below the saturated strength. This hints at a connection between X-ray activity and the topology of the magnetic field, with large-scale fields hosting high X-ray activity levels.

Large-scale, low-multipolar magnetic field components could extend the range of the stellar fields to significantly larger radii. We speculate that if coronae filled these large-scale fields, resulting in a larger X-ray emitting volume, the stars with significant large-scale fields would show higher X-ray activity levels than stars dominated by small-scale fields. This would help to keep X-ray activity near saturated levels despite the increasingly cool atmospheres. The large scatter in X-ray acitivity may, therefore, represent the varying strength of the large-scale stellar field components. The X-ray emission from stars with similar rotation velocities and spectral types (such as LHS 2065 and 2MASS J10481463-3956062) could be indicative of the relative topology of their magnetic fields.

Stars with large-scale fields could also be expected to exhibit generally slower rotational velocities. Although Gastine et al. (2013) found that large-and-small scale topologies can be generated in the same rotation regime, the rotational evolution may depend on the large-scale magnetic topologies. Spin-down or spin-up processes may be affected by the increased moment of inertia from an extended corona, and magnetic braking is believed to be more significant in large-scale fields than in tangled, high-multipolar fields (Reiners & Mohanty 2012). We speculate that stars with large-scale, dipolar fields may form with similar rotation values as low-activity, multipolar stars. As they evolve, stars with large-scale fields will spin-down more quickly, resulting in the observed anticorrelation between activity and rotation.

Little overlap exists between UCDs observed in X-ray and with measured magnetic topologies. Morin et al. (2010) finds that GJ 1245 B and VB 10 ($L_X/L_{bol} = -4.3$ and -5.1 in quiescence) both show no evidence of strong large-scale components, supportive of our speculation. VB 8 is also found to be dominated by small-

scale fields, although it shows higher quiescent activity ($L_X/L_{bol} = -3.5$). McLean et al. (2011) suggest that observed periodicities in radio emission in NLTT 33370 AB ($L_X/L_{bol} = -3.6$ in quiescence) suggest the existence of significant large-scale field components, although this has not been confirmed with ZDI observations. Further study is required to examine the connection between magnetic topology and coronal activity measurements in UCDs, although this is complicated by the difficulty of obtaining ZDI measurements of rapidly-rotating stars.

6. SUMMARY AND CONCLUSIONS

We have presented the most complete sample to date of ultracool dwarfs (M6.5 and later) with known rotational velocities and observations in X-ray wavelengths. Included in this sample are eight new observations from *Chandra*. We also have presented reductions of three late-type objects from the *Chandra* Data Archive, GJ 1245 AC (M5.5+M8.5, an unresolved tight binary), GJ 1245 B (M6.0), and 2MUCD 10158 (L8), while the reductions of the archival observation of LP 349–25 AB will be presented in Williams et al. (in prep.). Combining the eight newly observed UCDs and the archival observations with all objects available from the literature, our sample represents 33 objects later than M6. All of these UCDs are fast rotators ($P_{rot} \lesssim 1$ day) yet the majority show X-ray luminosity over an order of magnitude lower than predicted from their bolometric luminosities and the established activity-rotation relation for early-M dwarfs.

We find evidence for an anticorrelation between X-ray activity and rotation in the UCD sample, similar to the supersaturation effects observed in rapidly-rotating solar-type stars. However the X-ray activity of many UCDs is found to be orders of magnitude lower than in "supersaturated" solar-type stars, suggesting that UCDs do not represent the rapidly-rotating end of the same activity-rotation relations found in solar-type stars.

As radio activity was found by McLean et al. (2012) to increase with faster rotation even in the UCD regime, it is unlikely that this X-ray activity decrease is due to a decrease in the efficiency of the magnetic dynamo. Centrifugal stripping alone is also unlikely to be responsible, as the supersaturated UCDs would require extremely large corona for centrifugal effects to be significant. The overall scatter in quiescent activity between stars with similar spectral types and rotational velocities suggests that a separate parameter, correlated weakly with both rotation and X-ray activity, is required to match the observed trends.

We speculate that the magnetic field topology represents such a parameter, as large-scale field strengths in convective stars appear to correlate with rotation and spectral-type in a similar fashion to X-ray activity. Strong large-scale components may extend the coronal volume, increasing observed X-ray emissions. Stars in both the large-scale and small-scale field regimes may form with similar rotation periods, but large-scale, X-ray active stars will spin-down through enhanced magnetic braking, resulting in the observed anticorrelation. If true, the X-ray emissions of UCDs may only trace the large-scale components of magnetic fields rather than the integrated flux across large-and-small scales.

This framework does not offer a clear explanation for the observed trends in UCD radio activity, found by Berger et al. (2010) and McLean et al. (2012). There exist a substantial population of UCDs with strong radio activity but with X-ray activity levels below that predicted by the radio/X-ray relation. Yet some X-ray detected sources have yet to be detected in the radio as well. The breakdown of this correlation in the UCD regime will be addressed further in Williams et al. (in prep.).

Further observations are required to increase the number of UCDs with known magnetic topologies and X-ray fluxes, but we speculate that X-ray activity should be correlated with the large-scale fraction of the magnetic fields. Further ZDI measurements (performed in conjunction with X-ray observations) can help illuminate the effect of large-scale topology on coronal emissions. Obtaining an improved understanding of the radio properties of the fastest rotators should also be a high priority. The newly upgraded Karl G. Jansky Very Large Array, with its sensitivity increase of nearly an order of magnitude compared to the original system, offers an excellent opportunity to improve on previous work. In addition, theoretical models should continue to push into extremely-rapid rotation regimes, to provide accurate explanations for the trends being found observationally.

B. A. C. thanks Jonathan McDowell and Marie Machecek for their advice and comments on drafts of this work, as well as Scott Wolk for a helpful discussion on X-ray analysis and reductions. This work is supported in part by the National Science Foundation REU and Department of Defense ASSURE programs under NSF Grant no. 1262851 and by the Smithsonian Institution. E. B. and P. K. G. W. acknowledge support for this work from the National Science Foundation through Grant AST-1008361, and from the National Aeronautics and Space Administration through Chandra Award Number GO2-13007A issued by the Chandra X-ray Observatory Center, which is operated by the Smithsonian Astrophysical Observatory for and on behalf of the National Aeronautics Space Administration under contract NAS8-03060. This research has made use of data obtained from the *Chandra Data Archive* and the *Chandra Source Catalog*, as well as software provided by the *Chandra X-ray Center (CXC)* in the application packages *CIAO v4.5*, *ChIPS*, and *Sherpa*. This research has also made use of the SIMBAD database, operated at CDS, Strasbourg, France, and NASA's Astrophysics Data System.

APPENDIX

Table 6
Properties of X-ray active UCDs

Name	2MASS ID	SpT	State[a]	J[b] (mag)	K[b] (mag)	Distance (pc)	$v \sin i$ (km s^{-1})	Ref.	$\log F_X$ (erg s^{-1} cm^{-2})	Ref.	Orig. Band[c] keV	$\log L_X$ (erg s^{-1})	$\log(L_X/L_{bol})$
Newly observed UCDs – see Williams et al. (in prep.)													
LHS 292	10481258 − 1120082	M6.5		8.860	7.930	4.54	<3.0	2	-13.66	3	0.3-2.0	25.73	-4.70
LHS 523	22285440 − 1325178	M6.5		10.768	9.843	11.30	∼7.0	2	-12.66	3	0.3-2.0	27.53	-2.93
NLTT 33370 AB	13142039 + 1320011AB	M7	Fl.	9.750	8.790	16.40	45.0	2	-12.12	3	0.3-2.0	28.39	-2.80
...	...	...	Qu.	...	...	...	...	...	-12.88	3	0.3-2.0	27.63	-3.56
LP 851–346	11554286 − 2224586	M7.5	Fl.	10.930	9.880	9.70	33.0	2	-13.36	3	0.3-2.0	26.69	-3.57
...	...	...	Qu.	...	...	...	...	...	-14.26	3	0.3-2.0	25.79	-4.48
NLTT 40026	15210103 + 5053230	M7.5		12.010	10.920	16.10	40.0	2	-14.96	3	0.3-2.0	25.53	-4.75
LHS 2397a AB	11214924 − 1313084AB	M8+L7.5		11.930	10.730	14.30	15.0	2	-13.18	3	0.3-2.0	27.21	-3.02
LHS 3406	18432213 + 4040209	M8	Fl.	11.310	10.310	14.15	5.0	2	-13.36	3	0.3-2.0	27.02	-3.40
...	...	...	Qu.	...	...	...	...	...	-13.96	3	0.3-2.0	26.42	-4.01
LP 647–13	01095117 − 0343264	M9		11.690	10.430	11.10	13.0	2	-14.66	3	0.3-2.0	25.51	-4.59
Newly analyzed stars from *Chandra* archive													
GJ 1245 AC	19535443 + 4424541AC	M5.5+M8.5		7.791	6.854	4.55	22.5	2	-12.54	1	0.3-7.0	26.85	-4.03
GJ 1245 B	19535508 + 4424550B	M6.0	Fl.	8.287	7.387	4.55	6.8	2	-12.22	1	0.3-7.0	27.18	-3.49
...	...	...	Qu.	...	...	...	...	...	-12.99	1	0.3-7.0	26.40	-4.27
LP 349–25 AB	00275592 + 2219328AB	M8+M9	Fl.	10.610	9.570	10.30	55.0	2	-14.06	3	0.3-2.0	26.04	-4.40
...	...	...	Qu.	...	...	...	...	...	-14.66	3	0.3-2.0	25.45	-4.99
2MUCD 10158	02440357 − 4700509	L8		13.246	11.558	4.97	67.0	2	<-15.14	1	0.3-7.0	<24.33	<-4.68
UCDs with X-ray observations and $v \sin i$ from the literature													
LHS 248	08294949 + 2646348	M6.5		8.235	7.260	3.63	11.0	7	-12.67	16	0.1-2.4	26.52	-3.97
LHS 3003	14563831 − 2809473	M7		9.965	8.928	6.40	5.0	6	-13.47	16	0.1-2.4	26.23	-4.07
VB 8	16553529 − 0823401	M7	Fl.	9.776	8.816	6.50	9.0	6	-12.24	16	0.1-2.4	27.46	-2.91
...	...	...	Qu.	...	...	...	...	...	-12.82	13	0.1-2.4	26.88	-3.49
LP 412 31	03205965 + 1854233	M8	Fl.	11.759	10.639	14.51	15.0	6	-10.72	19	0.3-8.0	29.68	-0.62
...	...	...	Qu.	...	...	...	...	...	-13.19	19	0.3-8.0	27.21	-3.08
VB 10	19165762 + 0509021	M8	Fl.	9.908	8.765	6.10	6.5	7	-13.92	22	0.2-2.0	25.73	-4.56
...	...	...	Qu.	...	...	...	...	...	-14.43	22	0.2-2.0	25.22	-5.07
Gl569Ba	14542923 + 1606039A	M8.5	Fl.	11.270	10.160	9.80	19.0	9	-12.49	14	0.5-8.0	27.57	-2.57
...	...	...	Qu.	...	...	...	...	...	-14.22	14	0.5-8.0	25.84	-4.30
LSPM J1835+3259	18353790 + 3259545	M8.5		10.270	9.171	5.67	44.0	6	<-15.08	22	0.2-2.0	<24.51	<-5.55
LP-944 20	03393521 − 3525440	M9	Fl.	10.725	9.548	4.97	26.0	6	-13.92	20	0.1-10	25.55	-4.23
...	...	...	Qu.	...	...	...	...	...	<-15.44	20	0.1-10	<24.03	<-5.75
LHS 2065	08533619 − 0329321	M9	Fl.	11.212	9.942	8.50	13.5	6	-12.39	17	0.1-2.4	27.54	-2.52
...	...	...	Qu.	...	...	...	...	...	-13.42	18	0.3-0.8	26.52	-3.55
2MASS J10481463-3956062	10481463 − 3956062	M9		9.538	8.447	4.02	18.0	6	-14.18	12	0.2-2.0	25.10	-4.95
1RXS J115928.5-524717	11592743 − 5247188	M9	Fl.	11.430	10.322	10.20	25.0	4	-11.28	10	0.1-2.4	28.81	-1.29
...	...	...	Qu.	...	...	...	...	...	<-12.17	10	0.1-2.4	<27.93	<-2.18
TVLM 513-46546	15010818 + 2250020	M9		11.866	10.706	9.90	60.0	7	-15.16	24	0.3-2.0	24.91	-5.00
BRI B0021-0214	00242463 − 0158201	M9.5		11.992	10.539	12.10	33.0	6	<-15.10	23	0.2-2.0	<25.15	<-4.95
PC 0025+0447	00274197 + 0503417	M9.5		16.189	14.964	72.00	13.0	8	<-15.57	12	0.3-8.0	<26.22	<-3.70
2MASS J07464256+2000321 AB	07464256 + 2000321AB	L0.5		11.759	10.468	12.21	31.0	5	<-15.05	11	0.2-2.0	<25.21	<-5.00
LSR J0602+3910	06023045 + 3910592	L1.0		12.300	10.865	10.60	9.0	5	<-15.10	23	0.2-2.0	<25.03	<-4.88
Kelu-1 AB	13054019 − 2541059AB	L2		13.414	11.747	18.70	76.0	5	-15.28	15	0.1-10	25.34	-4.68
2MASSI J0523382-140302	05233822 − 1403022	L2.5		13.084	11.638	13.40	21.0	5	<-15.10	23	0.2-2.0	<25.24	<-4.53
LSPM J0036+1821	00361617 + 1821104	L3.5		12.466	11.058	8.76	45.0	5	<-15.02	21	0.2-8.0	<24.94	<-4.66
HD 130948b	14501581 + 2354424B	L4		12.600	11.000	17.90	62.0	9	<-15.22	14	0.5-8.0	<25.36	<-4.86
HD 130948c	14501581 + 2354424C	L4		12.900	11.300	17.90	86.0	9	<-15.22	14	0.5-8.0	<25.36	<-4.74
DENIS-P J1228.2-1547 AB	12281523 − 1547342AB	L5		14.378	12.767	20.20	22.0	7	<-14.07	12	0.3-8.0	<26.62	<-3.03
2MASSW J1507476-162738	15074769 − 1627386	L5		12.830	11.312	7.33	32.0	5	<-15.02	21	0.2-8.0	<24.79	<-4.57

Table 6 — *Continued*

Name	2MASS ID	SpT	State[a]	J[b] (mag)	K[b] (mag)	Distance (pc)	$v \sin i$ (km s^{-1})	Ref.	$\log F_X$ (erg s^{-1} cm^{-2})	Ref.	Orig. Band[c] keV	$\log L_X$ (erg s^{-1})	$\log(L_X/L_{bol})$

References. — [1] This Work, [2] see Table 1 , [3] Williams et al. (in prep.), [4] Robrade & Schmitt (2009), [5] Reiners & Basri (2008), [6] Reiners & Basri (2010), [7] Mohanty & Basri (2003), [8] McLean et al. (2012), [9] Konopacky et al. (2012), [10] Hambaryan et al. (2004), [11] Berger et al. (2009), [12] Stelzer et al. (2012), [13] Güdel et al. (1993), [14] Stelzer et al. (2006a), [15] Audard et al. (2007), [16] Schmitt et al. (1995), [17] Schmitt & Liefke (2002), [18] Robrade & Schmitt (2008), [19] Stelzer et al. (2006b), [20] Rutledge et al. (2000), [21] Berger et al. (2005), [22] Berger et al. (2008b), [23] Berger et al. (2010), [24] Berger et al. (2008a)

[a] Fl. and Qu. represent flaring and quiescent states, respectively, if both were observed for an object

[b] All J and K magnitudes from 2MASS Point Sources Catalog (Cutri et al. 2003), accessed using the SIMBAD database.

[c] Original band in which flux was measured. Listed fluxes and luminosities are converted to 0.2–2.0 keV band.

REFERENCES

Audard, M., Osten, R. A., Brown, A., et al. 2007, Astronomy and Astrophysics, 471, L63

Baraffe, I., Chabrier, G., Allard, F., & Hauschildt, P. 1998, Astronomy and Astrophysics, v.337, p.403-412 (1998), 15

Benz, A. O., & Güdel, M. 1994, Astronomy and Astrophysics 285, 621-630 (1994)

Berger, E., Ball, S., Becker, K. M., et al. 2001, Nature, Volume 410, Issue 6826, pp. 338-340 (2001)., 338

Berger, E., Rutledge, R. E., Reid, I. N., et al. 2005, The Astrophysical Journal, 627, 960

Berger, E., Gizis, J. E., Giampapa, M. S., et al. 2008a, The Astrophysical Journal, 673, 1080

Berger, E., Basri, G., Gizis, J. E., et al. 2008b, The Astrophysical Journal, 676, 1307

Berger, E., Rutledge, R. E., Phan-Bao, N., et al. 2009, The Astrophysical Journal, 695, 310

Berger, E., Basri, G., Fleming, T. A., et al. 2010, The Astrophysical Journal, 709, 332

Browning, M. K. 2008, The Astrophysical Journal, 676, 1262

Chabrier, G., & Baraffe, I. 1997, Astronomy and Astrophysics, v.327, p.1039-1053 (1997), arXiv:9704118 [astro-ph]

Chabrier, G., & Küker, M. 2006, Astronomy and Astrophysics, 446, 1027

Costa, E., Méndez, R. A., Jao, W.-C., et al. 2006, The Astronomical Journal, 132, 1234

Cram, L. E. 1982, The Astrophysical Journal, 253, 768

Cranmer, S. R., & Saar, S. H. 2011, The Astrophysical Journal, 741, 54

Crifo, F., Phan-Bao, N., Delfosse, X., et al. 2005, Astronomy and Astrophysics, 441, 653

Cruz, K. L., Reid, I. N., Liebert, J., Kirkpatrick, J. D., & Lowrance, P. J. 2003, The Astronomical Journal, 126, 2421

Cruz, K. L., Reid, I. N., Kirkpatrick, J. D., et al. 2007, The Astronomical Journal, 133, 439

Cutri, R. M., Skrutskie, M. F., van Dyk, S., et al. 2003, VizieR Online Data Catalog, 2246

Deacon, N. R., Hambly, N. C., & Cooke, J. A. 2005, Astronomy and Astrophysics, 435, 363

Delfosse, X., Forveille, T., Perrier, C., & Mayor, M. 1998, Astronomy and Astrophysics, v.331, p.581-595 (1998)

Delfosse, X., Forveille, T., Ségransan, D., et al. 2000, Astronomy and Astrophysics, v.364, p.217-224 (2000), arXiv:0010586 [astro-ph]

Donati, J.-F., Forveille, T., Cameron, A. C., et al. 2006, Science (New York, N.Y.), 311, 633

Donati, J.-F., Morin, J., Petit, P., et al. 2008, Monthly Notices of the Royal Astronomical Society, 390, 545

Durney, B. R., Young, D. S., & Roxburgh, I. W. 1993, Solar Physics, 145, 207

Feigelson, E. D., & Babu, G. J. 2012, Modern Statistical Methods for Astronomy (Cambridge University Press)

Forbrich, J., Wolk, S. J., Güdel, M., et al. 2011, 16th Cambridge Workshop on Cool Stars, 448

Forveille, T., Beuzit, J.-L., Delorme, P., et al. 2005, Astronomy and Astrophysics, 435, L5

Freed, M., Close, L. M., & Siegler, N. 2003, The Astrophysical Journal, 584, 453

Freeman, P., Doe, S., & Siemiginowska, A. 2001, in Proc. SPIE Vol. 4477, ed. J.-L. Starck & F. D. Murtagh, Vol. 4477, 76

Fruscione, A., McDowell, J. C., Allen, G. E., et al. 2006, in Observatory Operations: Strategies, ed. D. R. Silva & R. E. Doxsey, Vol. 6270, 62701V

Gastine, T., Morin, J., Duarte, L., et al. 2013, Astronomy & Astrophysics, 549, L5

Gizis, J. E., Monet, D. G., Reid, I. N., et al. 2000, The Astronomical Journal, 120, 1085

Gregory, P. C., & Loredo, T. J. 1992, The Astrophysical Journal, 398, 146

Güdel, M. 2002, Annual Review of Astronomy and Astrophysics, 40, 217

Güdel, M., & Benz, A. O. 1993, The Astrophysical Journal, 405, L63

Güdel, M., Benz, A. O., Schmit, J. H. M. M., & Skinner, S. L. 1996, The Astrophysical Journal, 471, 1002

Güdel, M., Schmitt, J. H. M. M., Bookbinder, J. A., & Fleming, T. A. 1993, The Astrophysical Journal, 415, 236

Guenther, E. W., & Wuchterl, G. 2003, Astronomy and Astrophysics, 401, 677

Hambaryan, V., Staude, A., Schwope, A. D., et al. 2004, Astronomy and Astrophysics Astrophysics, 415, 265

Harrington, R. S., & Dahn, C. C. 1984, IAU Circ., 3989, 1 (1984). Edited by Marsden, B. G.

Hawley, S. L., Gizis, J. E., & Reid, I. N. 1996, The Astronomical Journal, 112, 2799

Helsel, D. R. 2005, Nondetects and data analysis: statistics for censored environmental data, Statistics in practice (Wiley-Interscience)

Henry, T. J., Kirkpatrick, J. D., & Simons, D. A. 1994, The Astronomical Journal, 108, 1437

Henry, T. J., Walkowicz, L. M., Barto, T. C., & Golimowski, D. A. 2002, The Astronomical Journal, 123, 2002

James, D. J., Jardine, M. M., Jeffries, R. D., et al. 2000, Monthly Notices of the Royal Astronomical Society, 318, 1217

Jardine, M. 2004, Astronomy and Astrophysics, 414, L5

Jardine, M., & Unruh, Y. C. 1999, Astronomy and Astrophysics, v.346, p.883-891 (1999)

Jenkins, J. S., Ramsey, L. W., Jones, H. R. A., et al. 2009, The Astrophysical Journal, 704, 975

Kiraga, M., & Stępień, K. 2007, Acta Astronomica, Vol. 57, pp.149-172, 20

Kirkpatrick, J. D., Henry, T. J., & McCarthy, D. W. 1991, The Astrophysical Journal Supplement Series, 77, 417

Kirkpatrick, J. D., Cruz, K. L., Barman, T. S., et al. 2008, The Astrophysical Journal, 689, 1295

Konopacky, Q. M., Ghez, A. M., Fabrycky, D. C., et al. 2012, The Astrophysical Journal, 750, 79

Kraft, R. P., Burrows, D. N., & Nousek, J. A. 1991, The Astrophysical Journal, 374, 344

Küker, M., & Rüdiger, G. 1999, Astronomy and Astrophysics, v.346, p.922-928 (1999)

Law, N. M., Hodgkin, S. T., & Mackay, C. 2006, Monthly Notices of the Royal Astronomical Society, 368, 1917

Law, N. M., Hodgkin, S. T., & Mackay, C. D. 2008, Monthly Notices of the Royal Astronomical Society, 384, 150

Lépine, S., Thorstensen, J. R., Shara, M. M., & Rich, R. M. 2009, The Astronomical Journal, 137, 4109

Luhman, K. L., Stauffer, J. R., Muench, A. A., et al. 2003, The Astrophysical Journal, 593, 1093

Luyten, W. J. 1976, Univ. Minnesota

—. 1979, New Luyten catalogue of stars with proper motions larger than two tenths of an arcsecond; and first supplement; NLTT. (Minneapolis (1979)); Label 12 = short description; Label 13 = documentation by Warren; Label 14 = catalogue, Strasbour

McLean, M., Berger, E., Irwin, J., Forbrich, J., & Reiners, A. 2011, The Astrophysical Journal, 741, 27

McLean, M., Berger, E., & Reiners, A. 2012, The Astrophysical Journal, 746, 23

Mohanty, S., & Basri, G. 2003, The Astrophysical Journal, 583, 451

Mohanty, S., Basri, G., Shu, F., Allard, F., & Chabrier, G. 2002, The Astrophysical Journal, 571, 469

Morin, J., Donati, J.-F., Petit, P., et al. 2010, Monthly Notices of the Royal Astronomical Society, 407, 2269

Morin, J., Dormy, E., Schrinner, M., & Donati, J.-F. 2011, Monthly Notices of the Royal Astronomical Society: Letters, 418, L133

Morin, J., Donati, J.-F., Petit, P., et al. 2008, Monthly Notices of the Royal Astronomical Society, 390, 567

Muirhead, P. S., Hamren, K., Schlawin, E., et al. 2012, The Astrophysical Journal, 750, L37

Nakajima, T., Tsuji, T., & Yanagisawa, K. 2004, The Astrophysical Journal, 607, 499

Neupert, W. M. 1968, The Astrophysical Journal, 153, L59

Noyes, R. W., Hartmann, L. W., Baliunas, S. L., Duncan, D. K., & Vaughan, A. H. 1984, The Astrophysical Journal, 279, 763

Parker, E. N. 1955, The Astrophysical Journal, 122, 293
Pizzolato, N., Maggio, A., Micela, G., Sciortino, S., & Ventura, P. 2003, Astronomy and Astrophysics, 397, 147
Randich, S. 1998, ASP Conf. Ser. 154, The Tenth Cambridge Workshop on Cool Stars, Stellar Systems and the Sun, Edited by R. A. Donahue and J. A. Bookbinder, p.501, 9
Randich, S., Schmitt, J. H. M. M., Prosser, C. F., & Stauffer, J. R. 1996, Astronomy and Astrophysics, v.305, p.785
Reiners, A., & Basri, G. 2006, The Astrophysical Journal, 644, 497
—. 2008, The Astrophysical Journal, 684, 1390
—. 2009, Astronomy and Astrophysics, 496, 787
—. 2010, The Astrophysical Journal, 710, 924
Reiners, A., & Mohanty, S. 2012, The Astrophysical Journal, 746, 43
Robrade, J., & Schmitt, J. H. M. M. 2008, Astronomy and Astrophysics, 487, 1139
—. 2009, Astronomy and Astrophysics, 496, 229
Rutledge, R. E., Basri, G., Martín, E. L., & Bildsten, L. 2000, The Astrophysical Journal, 538, L141
Scargle, J. D., Norris, J. P., Jackson, B., & Chiang, J. 2013, The Astrophysical Journal, 764, 167
Schmitt, J. H. M. M., Fleming, T. A., & Giampapa, M. S. 1995, The Astrophysical Journal, 450, 392
Schmitt, J. H. M. M., & Liefke, C. 2002, Astronomy and Astrophysics, 382, L9
—. 2004, Astronomy and Astrophysics, 417, 651
Semel, M. 1989, Astronomy and Astrophysics (ISSN 0004-6361), vol. 225, no. 2, Nov. 1989, p. 456-466.
Skumanich, A. 1972, The Astrophysical Journal, 171, 565
Stelzer, B., Micela, G., Flaccomio, E., Neuhäuser, R., & Jayawardhana, R. 2006a, Astronomy and Astrophysics, 448, 293
Stelzer, B., Schmitt, J. H. M. M., Micela, G., & Liefke, C. 2006b, Astronomy and Astrophysics, 460, L35
Stelzer, B., Alcalá, J., Biazzo, K., et al. 2012, Astronomy and Astrophysics, 537, A94
Stępień, K., Schmitt, J. H. M. M., & Voges, W. 2001, Astronomy and Astrophysics, 370, 157
van Altena, W. F., Lee, J. T., & Hoffleit, E. D. 1995, New Haven
Vilhu, O. 1984, Astronomy and Astrophysics (ISSN 0004-6361), vol. 133, no. 1, April 1984, p. 117-126.
Voges, W., Aschenbach, B., Boller, T., et al. 1999, Astronomy and Astrophysics, v.349, p.389-405 (1999), arXiv:9909315 [astro-ph]
West, A. A., Hawley, S. L., Bochanski, J. J., et al. 2008, The Astronomical Journal, 135, 785
West, A. A., Hawley, S. L., Walkowicz, L. M., et al. 2004, The Astronomical Journal, 128, 426
Wilking, B. A., Greene, T. P., & Meyer, M. R. 1999, The Astronomical Journal, 117, 469
Williams, P. K. G., et al. in prep.
Wright, N. J., Drake, J. J., Mamajek, E. E., & Henry, G. W. 2011, The Astrophysical Journal, 743, 48